Faculty Bibliography 2010s

Faculty Bibliography

1-1-2011

The production of Titan's ultraviolet nitrogen airglow

Michael H. Stevens

Jacques Gustin

Joseph M. Ajello

J. Scott Evans

R. R. Meier

See next page for additional authors

Find similar works at: https://stars.library.ucf.edu/facultybib2010
University of Central Florida Libraries http://library.ucf.edu

Recommended Citation

Authors

Michael H. Stevens, Jacques Gustin, Joseph M. Ajello, J. Scott Evans, R. R. Meier, Andrew J. Kochenash, Andrew W. Stephan, A. Ian F. Stewart, Larry W. Esposito, William E. McClintock, Greg Holsclaw, E. Todd Bradley, B. R. Lewis, and A. N. Heays

The production of Titan's ultraviolet nitrogen airglow

Michael H. Stevens,[1] Jacques Gustin,[2] Joseph M. Ajello,[3] J. Scott Evans,[4] R. R. Meier,[5]
Andrew J. Kochenash,[4] Andrew W. Stephan,[1] A. Ian F. Stewart,[6] Larry W. Esposito,[6]
William E. McClintock,[6] Greg Holsclaw,[6] E. Todd Bradley,[7] B. R. Lewis,[8]
and A. N. Heays[8]

[1] The Cassini Ultraviolet Imaging Spectrograph (UVIS) observed Titan's dayside limb in the extreme ultraviolet (EUV) and far ultraviolet (FUV) on 22 June 2009 from a mean distance of 23 Titan radii. These high-quality observations reveal the same EUV and FUV emissions arising from photoelectron excitation and photofragmentation of molecular nitrogen (N_2) as found on Earth. We investigate both of these solar driven processes with a terrestrial airglow model adapted to Titan and find that total predicted radiances for the two brightest N_2 band systems agree with the observed peak radiances to within 5%. Using N_2 densities constrained from in situ observations by the Ion Neutral Mass Spectrometer on Cassini, the altitude of the observed limb peak of the EUV and FUV emission bands is between 840 and 1060 km and generally consistent with model predictions. We find no evidence for carbon emissions in Titan's FUV airglow in contrast to previous Titan airglow studies using UVIS data. In their place, we identify several vibrational bands from the N_2 Vegard-Kaplan system arising from photoelectron impact with predicted peak radiances in agreement with observations. These Titan UV airglow observations are therefore comprised of emissions arising only from solar processes on N_2 with no detectable magnetospheric contribution. Weaker EUV Carroll-Yoshino N_2 bands within the $v' = 3$, 4, and 6 progressions between 870 and 1020 Å are underpredicted by about a factor of five while the (0,1) band near 980 Å is overpredicted by about a factor of three.

Citation: Stevens, M. H., et al. (2011), The production of Titan's ultraviolet nitrogen airglow, *J. Geophys. Res.*, *116*, A05304, doi:10.1029/2010JA016284.

1. Introduction

[2] The observed extreme ultraviolet (EUV, 600–1150 Å) and far ultraviolet (FUV, 1150–1900 Å) airglow of Titan contains a wealth of information on solar driven processes involving molecular nitrogen (N_2). The first observations of Titan's UV airglow were made 30 years ago by the Voyager 1 Ultraviolet Spectrometer (UVS) [*Broadfoot et al.*, 1981].

Early analysis of these data indicated that magnetospheric electrons controlled the EUV and FUV airglow production due largely to the identification of the readily excited N_2 Carroll-Yoshino (CY) c'_4 $^1\Sigma_u^+ - X^1\Sigma_g^+$ (0,0) band near 958 Å, which is optically thick near peak photoelectron production [*Strobel and Shemansky*, 1982]. But ensuing studies of the observed EUV limb profile shape indicated that magnetospheric electron excitation contributed less than 10% to the signal and that photoelectron excitation dominated [*Strobel et al.*, 1991; *Gan et al.*, 1992]. *Stevens* [2001] argued that CY(0,0) was misidentified and suggested that the UVS EUV airglow observations could be explained exclusively by photoelectron excitation and photofragmentation of N_2 producing blended N I multiplets. However, the low UVS spectral resolution (~30 Å) and uncertainties in the UVS EUV calibration (50%) [*Strobel et al.*, 1992] prevented a definitive answer to these lingering questions.

[3] Now the Cassini Ultraviolet Imaging Spectrograph (UVIS) has made high-quality observations of Titan at a spectral resolution over five times better than the Voyager UVS. Study of the EUV UVIS disk observations from December 2004 confirmed the absence of the CY(0,0) band

[1]Space Science Division, Naval Research Laboratory, Washington, D. C., USA.

[2]Laboratoire de Physique Atmosphérique et Planétaire, Université de Liège, Liège, Belgium.

[3]Jet Propulsion Laboratory, California Institute of Technology, Pasadena, California, USA.

[4]Computational Physics, Inc., Springfield, Virginia, USA.

[5]Department of Physics and Astronomy, George Mason University, Fairfax, Virginia, USA.

[6]Laboratory for Atmospheric and Space Physics, University of Colorado at Boulder, Boulder, Colorado, USA.

[7]Department of Physics, University of Central Florida, Orlando, Florida, USA.

[8]Research School of Physics and Engineering, Australian National University, Canberra, ACT, Australia.

with N I multiplets present instead [*Ajello et al.*, 2007] and also revealed features in the FUV that were reported to be from carbon (C I) [*Ajello et al.*, 2008; *Zhang et al.*, 2010]. A comparison of the integrated EUV and FUV N_2 airglow disk emission observed by UVS and UVIS roughly varies as the solar X-ray ultraviolet (XUV, $\lambda < 450$ Å) [*Ajello et al.*, 2007, 2008] and these disk observations were recently modeled by *Lavvas et al.* [2011]. However, a systematic comparison of the many electronic and vibrational transitions observed on the limb by UVIS with predictions from an airglow model containing the relevant excitation processes has not yet been done. The altitude of peak emission and the shape of the profiles are particularly important in quantifying the solar driven contribution to the Titan airglow and a comparison of observed EUV and FUV limb profiles with model predictions is critical to this end.

[4] The purpose of this work is to quantitatively understand the EUV and FUV spectral content of Titan's atmosphere and to model the limb radiances for each set of emissions observed. We first establish the spectral content of the Titan EUV and FUV airglow using high-quality UVIS EUV and FUV limb observations between 750 and 1250 km tangent altitudes. We then adapt an airglow radiance model developed for the terrestrial atmosphere to Titan, calculate vertical profiles of volume production rates (VPRs) for the features observed by UVIS, and compare predicted limb radiances with the observations. Finally, we discuss our results in the context of previous terrestrial airglow observations, the latest laboratory observations of N_2, and future UVIS airglow observations of Titan.

2. The UVIS Limb Observations

[5] The UVIS is a two-channel imaging spectrograph that consists of an EUV channel (561–1182 Å) and a FUV channel (1115–1913 Å). The detector is a CODACON (CODed Anode array CONverter), with 1024 pixels in the spectral dimension and 64 pixels in the spatial dimension. The low-resolution slit was used for both channels, yielding a spectral resolution throughout the EUV and FUV of 4–6 Å. The rectangular field of view of the slit is 2×59 mrad in the EUV and 1.5×60 mrad in the FUV.

[6] The primary standards used for determining the UVIS absolute radiometric sensitivity prior to launch were photodiodes provided by the National Institute for Standards and Technology (NIST). NIST diodes were used to determine the absolute sensitivity of two LASP standards, a pulse counting Hamamatsu 1081 photomultiplier tube with a CsI photocathode and a pulse counting MCP detector. These standards were then used to calibrate the UVIS. Measurements of the star Alpha Virginis (Spica) obtained during cruise (16–17 January 1999) agreed with previous results [*Brune et al.*, 1979] to within 10% for both EUV and FUV channels, validating the UVIS laboratory results. Periodic stellar calibrations (every 100 days on average since 2006) obtained during cruise and while in orbit are used to track changes in UVIS sensitivity. From these stellar observations we estimate the UVIS calibration uncertainty to be 15% or better for all wavelengths. A discussion of the UVIS instrument characteristics can be found in the work of *Esposito et al.* [2004] and a discussion of the first EUV and FUV observations of Titan's disk from 13 December 2004

(Cassini Orbit TB) may be found in the work of *Ajello et al.* [2007, 2008].

[7] Data from the Titan encounter from 22 June 2009 (Orbit T57) used herein were obtained at a range of ~60,000 km (~23 Titan radii) and collected over a period of 60 min in 15 separate time steps by way of a unique "stare" observational mode employed for the first time. This mode compensated for spacecraft motion by repositioning the UVIS optical axis so that the central pixels of the UVIS slit were maintained at near 800 km minimum ray height as shown in Figure 1. This staring sequence allowed, to our knowledge, the highest S/N observation to date in both the EUV and FUV of the Titan airglow layer and a total of 888 spectra were obtained. Figure 1 shows UVIS FUV radiances integrated between 1250 and 1900 Å for each spectrum plotted against latitude and altitude. The vaguely parabolic relationship between latitude and altitude in Figure 1 is due to the rectangular field of view of the UVIS slit projected onto a fixed tangent altitude rather than by scanning in altitude. Overplotted are the projected spatial dimensions of three of the FUV pixels in order to convey the spatial resolution in altitude and latitude associated with a single spectrum. Each FUV pixel subtends 90 km in altitude (1.5 mrad) and each EUV pixel subtends 120 km in altitude (2.0 mrad).

[8] The uncertainty in pointing the UVIS slit at a fixed tangent altitude can be divided into two components. The first is the knowledge derived from pointing vectors after the observations, which is ± 0.14 mrad (J. Spitale, personal communication, 2011) or ± 8 km. The second is the stability of maintaining that tangent altitude during each 4 min integration. We estimate this stability by comparing the tangent altitudes determined at the beginning, middle, and end of each integration period. Taking the standard deviation of these altitudes at all spatial pixels over all 15 integrations and referencing them to the tangent altitude at the middle of each period, we find this uncertainty to be ± 23 km. This gives a quadratic sum of ± 24 km for the total pointing knowledge of one 4 min integration.

[9] The spectral region used in Figure 1 is dominated by the photoelectron excited N_2 Lyman-Birge-Hopfield (LBH) $a^1\Pi_g - {}^1X_g^+$ band system [*Ajello et al.*, 2008]. One can see that the LBH limb radiances peak near 900 km altitude and are smaller above and below this peak. The T57 observation spanned tangent altitudes from 750 km to 1350 km, and the associated spectra in Figure 1 are all from high enough altitudes that they do not exhibit significant emission from scattered sunlight.

[10] To maximize the signal-to-noise of the spectra, we collect all of our results in 100 km altitude bins centered on every 100 km increment from 800 to 1300 km. For the absolute uncertainty of the peak emission altitude we use the quadratic sum of the pointing knowledge uncertainty (± 24 km) and the size of the altitude bin (± 50 km), leading to a total of ± 55 km.

3. Spectral Analysis

3.1. FUV Emissions From Processes Involving N_2

[11] The first step of our analysis is to identify the spectral content of the airglow and derive limb brightness profiles of the main emission sources. *Ajello et al.* [2008] presented the first FUV airglow observations of UVIS from Titan's disk.
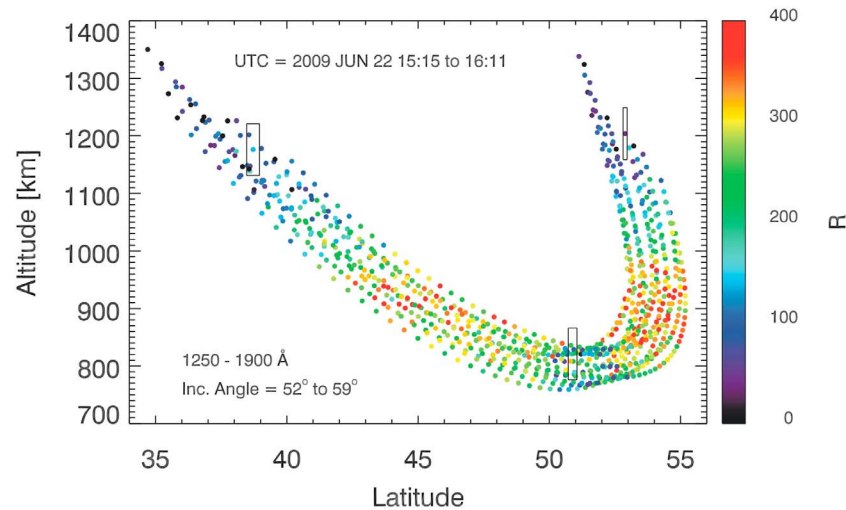
Figure 1. A scatterplot of the locations of each of the FUV spectra from the 15 time steps used in this study. There are a total of 888 separate spectra collected, and solar incidence angles vary slowly during the observations as indicated. The integrated radiance for the 1250–1900 Å spectral region is shown, which is primarily from the N_2 LBH bands. Also shown are the vertical and horizontal dimensions for three of the pixels projected to the minimum tangent height during one of the time steps. The projected vertical resolution of a single FUV pixel is ±45 km.

These observations showed that the FUV was dominated by LBH, N I multiplets produced by photofragmentation and photoelectron impact on N_2, the bright H Lyman-α line at 1216 Å, and solar scattered light modified by aerosol scattering and hydrocarbon absorption longward of ~1350 Å. In addition, Ajello et al. assigned features at 1464 Å, 1561 Å, and 1657 Å to C I from CH_4 fragmentation and identified a "mystery" feature at 1597 Å.

[12] We note two important advances from the earlier spectral analysis of *Ajello et al.* [2008]. First, by analyzing limb spectra at altitudes above 750 km, we avoid the difficulty of separating the relatively bright solar scattered signal originating from deeper in the atmosphere, which contributes to the disk observations longward of 1350 Å. Second, we find that the photoelectron excited N_2 Vegard-Kaplan (VK) $A^3\Sigma_u^+ - X^1\Sigma_g^+$ system is present longward of 1550 Å. The presence of N_2 VK bands in the Titan airglow has not been reported heretofore, but there are relatively bright VK bands close to the C I wavelengths at 1561 Å and 1657 Å as well as the unidentified feature at 1597 Å noted by *Ajello et al.* [2008].

[13] Our spectral analysis of the FUV limb spectra uses a least squares fitting procedure that includes all detectable emission between 1150 and 1900 Å. Each of these emissions is calculated at high spectral resolution and then convolved with the UVIS instrument line shape. These emissions include the following.

[14] 1. First is the H Lyman-α line at 1216 Å. The spectral width of this bright feature is found to be slightly larger than the other features in the Titan airglow. We therefore degrade the resolution of this feature slightly so that its full-width at half-maximum is 7 Å rather than 5 Å. This effect is consistent with an uncorrected loss in sensitivity at the core of the line due to persistent exposure by the interplanetary hydrogen background.

[15] 2. Second is the N_2 LBH system. The synthesis of this system uses the formalism described by *Conway* [1982] and each vibrational band is modeled using a rotational structure with a Boltzmann distribution at 170 K, consistent with temperatures reported for Titan's upper atmosphere [*De La Haye et al.*, 2007a].

[16] 3. Third is the N_2 VK system. We use upper state (v′ = 0–10) vibrational populations of *Strickland et al.* [1999] and extrapolate to a population of v′ = 11 that is 44% of that for v′ = 10. Branching ratios are from *Piper* [1993] and *Shemansky* [1969]. Electronic and vibrational energies as well as rotational constants are from *Huber and Herzberg* [1979] and the rotational structure is modeled at 170 K.

[17] 4. Fourth are the N I multiplets. These features are produced primarily by photofragmentation of N_2 with a smaller contribution from photoelectron excitation of N_2. Photofragmentation is also sometimes referred to as photodissociative excitation or photodissociative ionization, but we use the more general term here for simplicity. We use the relative intensities of the ten N I multiplets within the UVIS FUV passband, which are obtained from terrestrial airglow observations of the Hopkins Ultraviolet Telescope and reported by *Bishop and Feldman* [2003]. All atomic multiplets in the FUV are modeled as a single emission feature.

[18] We further note that there is significant extinction due to methane (CH_4) between 800 and 1300 km tangent altitudes for wavelengths shortward of 1400 Å [e.g., *Strobel et al.*, 1992] due to the large CH_4 absorption cross section at these wavelengths. There are two bright N I multiplets on either side of this absorption ledge, N I 1200 Å and N I 1493 Å, and the optically thin N I 1200 Å/1493 Å ratio is 2.8 [*Bishop and Feldman*, 2003]. The ratio of these features therefore can constrain the amount of CH_4 along the line-of-sight and so we include a fifth free variable in our spectral

fitting procedure which is the effective CH_4 slant column abundance observed on the limb. This column is only used to attenuate the different components of the spectral fit for a reliable determination of emergent radiances. We will discuss the sensitivity of the Titan airglow observations to the CH_4 abundance further in section 6.

[19] Each FUV spectrum is therefore fit using the following expression:

$$
\begin{aligned}
D(\lambda, z) = \big[& A_1(z)f_{Ly-\alpha}(\lambda) \\
& + A_2(z)f_{LBH}(\lambda) + A_3(z)f_{VK}(\lambda) + A_4(z)f_{NI}(\lambda) \big] \\
& \cdot \exp[-N_{CH4}(z)\sigma_{CH4}(\lambda)]
\end{aligned} \tag{1}
$$

where $D(\lambda, z)$ are the data for minimum tangent ray height z, $f_{Ly-\alpha}(\lambda)$ is the spectral shape of the H Lyman-α line, $f_{LBH}(\lambda)$ is the shape of the N_2 LBH bands, $f_{VK}(\lambda)$ is the shape of the N_2 VK bands, $f_{NI}(\lambda)$ is the shape of the N I multiplets, and $\sigma_{CH4}(\lambda)$ is the wavelength-dependent CH_4 absorption cross section [*Lee et al.*, 2001]. $N_{CH4}(z)$ (the effective CH_4 slant column abundance) and $A_n(z)$ are altogether the five least squares best fit coefficients of their corresponding linearly independent spectral components to the coaveraged data in each 100 km altitude bin. We use the synthetic fit to each spectral component to calculate the radiance contributions at each altitude. A nonlinear least squares fitting procedure was used, which also provided a relative fitting uncertainty for each altitude.

[20] Figures 2a–2d show the results of this spectral fitting procedure at the observed tangent altitude of 1000 ± 50 km, near the FUV emission peak. Figure 2a shows the composite solution overplotted on the data and the fit is excellent. Also included in Figure 2a is the best fit of the CH_4 transmission, referenced to the right-hand axis. The transmission on the short wavelength side of the spectrum is about 60%, whereas it is 100% on the long wavelength side of the spectrum due to the variation of the absorption cross section discussed above.

[21] Figures 2b–2d show the three components of the composite fit overplotted on the same data shown in Figure 2a. Figure 2b shows the best fit to the N_2 LBH bands. These bands constitute most of the N_2 emission in the FUV channel and are nearly optically thin, with only a small amount of CH_4 extinction on the short wavelength end of the system. The various band progressions are indicated and the observed radiance is 107.6 ± 12.1 R, which represents 87% of the emission within the entire LBH system (1260–2600 Å).

[22] Figure 2c shows the first identification of the N_2 VK bands in Titan's atmosphere. There is far more (95%) VK emission longward of 1900 Å [e.g., *Broadfoot et al.*, 1997], but we compare only the emission within the examined 1150–1900 Å spectral region (57.5 ± 7.4 R) against model predictions. The optically thin band progressions are indicated with the (7,0) band near 1689 Å being the brightest. This band and many other VK bands were obscured by the bright solar scattered background in the disk spectrum of *Ajello et al.* [2008]. Other bands clearly present in the blended limb spectrum are the (5,0), (6,0), (8,0), and (9,0). It is therefore very likely that the (8,0) band near 1654 Å as well as the weaker (11,0) band near 1563 Å were misidentified as C I by Ajello et al. and the (10,0) band near 1592 Å is likely the reported "mystery" feature. All three of

these features are within 5 Å of those considered by Ajello et al. We find no evidence of a third C I feature near 1464 Å in Figure 2a as reported by Ajello et al. We attempted to fit the brightest reported C I feature at 1657 Å to the data and found no detectable emission there, as suggested by the quality of the composite fit in Figure 2a. We place an upper limit of 2 R on this feature at 1000 km tangent altitude.

[23] Figure 2d shows the relative intensities of the N I multiplets produced primarily from photodissociative excitation ($h\nu + N_2$) with a smaller contribution from photoelectron excitation ($e^- + N_2$) [*Bishop and Feldman*, 2003]. Note that the N I 1200 Å/N I 1493 Å ratio is about 2 rather than the optically thin ratio of 2.8 as a consequence of CH_4 extinction. Other N I multiplets are labeled by tick marks. The total N I radiance within the spectral region shown is 27.3 ± 3.7 R. We therefore conclude that only features belonging to processes involving N_2 are present in the FUV (>1216 Å).

3.2. EUV Emissions and the N_2 Carroll-Yoshino System

[24] Our approach to the spectral analysis of the EUV airglow is analogous to that for the FUV in that we assemble the principal components to the blended spectrum and find a least squares best fit solution at each altitude. Rather than fit an EUV laboratory spectrum resulting from electron impact on N_2 to the data (as in the work of *Ajello et al.* [2007]), we fit the features separately where possible so that we can identify the largest discrepancies when comparing with model simulations. If there are many weak features within a progression (i.e., arising from the same upper state), then we fit the relative intensities of the entire progression together instead.

[25] The EUV limb spectra are fit between 750 and 1150 Å and all of the features are convolved with the UVIS instrument line shape before inclusion into the least squares fitting algorithm. The different spectral components are listed here.

[26] 1. The first component is the CY(0,v'') bands. The (0,0) and (0,1) bands near 958 and 980 Å, respectively, are fit together but we use the (0,1)/(0,0) ratio of 40 calculated under limb viewing conditions from a multiple scattering model [*Stevens*, 2001], thereby rendering negligible the contribution from the optically thick (0,0), as observed [*Ajello et al.*, 2007]. The (0,2) band near 1003 Å is fit separately and the (0,$v'' > 2$) bands are weak and not included. In contrast to the LBH and VK bands, the rotational structure of the CY bands is not explicitly included in the spectral fitting because the UVIS spectral resolution (~5 Å) is much broader than the width of the bands (~1 Å).

[27] 2. The second component is the CY($v' = 3,4,6$) bands. Since these bands are relatively weak and blended, all three of these progressions are fit together as one spectral component. Relative intensities within the blended features are obtained using emission cross sections of *Ajello et al.* [1989, 1998]. Bands terminating on the ground vibrational state are assumed to be optically thick and not included in the fit.

[28] 3. The third component is the N I and N II multiplets. As in the FUV, these features are produced primarily by photofragmentation of N_2. There are a total of 16 atomic multiplets within the UVIS EUV spectral region. The
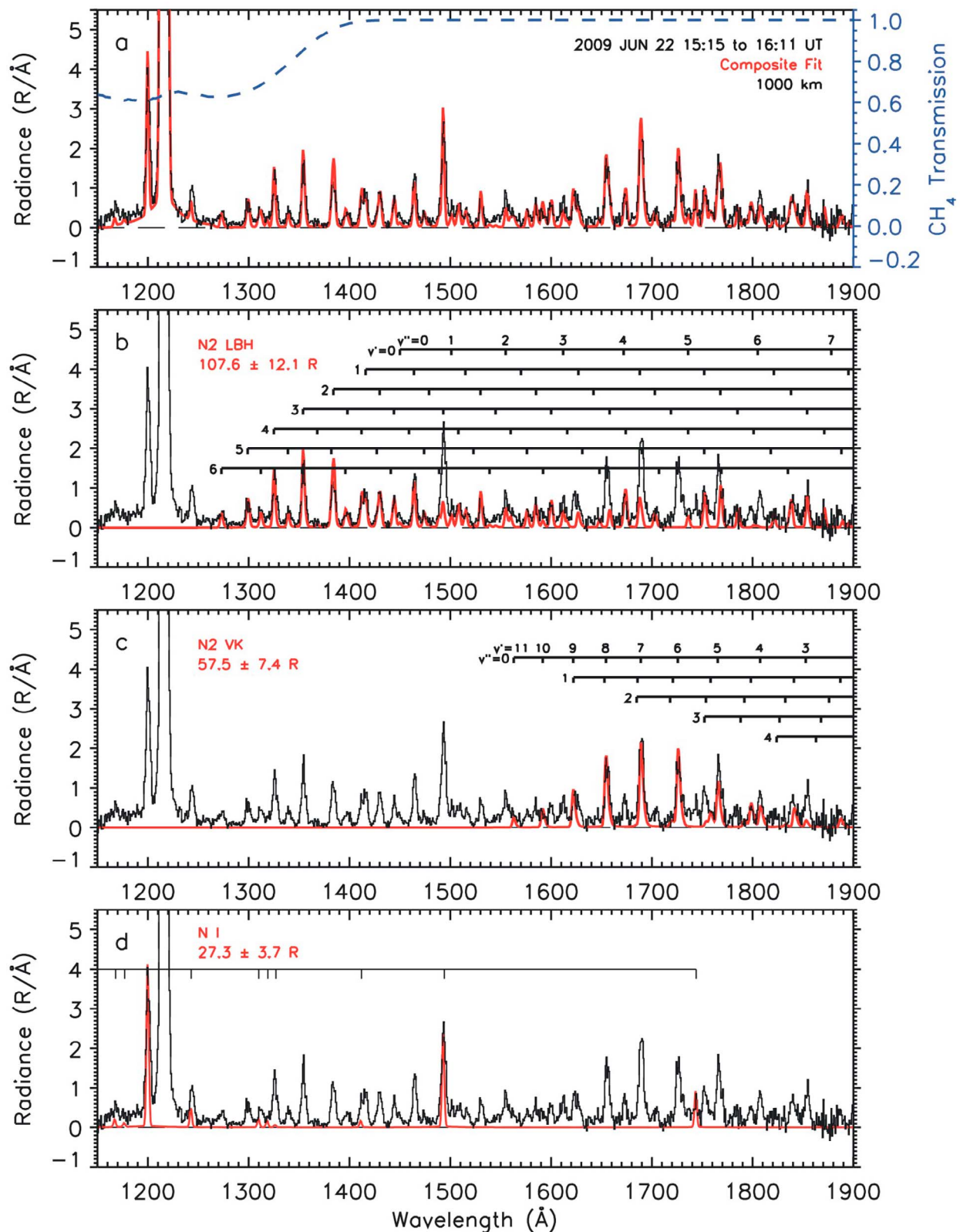
Figure 2. (a) UVIS FUV data from 22 June 2009 at 1000 ± 50 km altitude, where a total of 163 spectra have been coaveraged. The composite fit to the data is shown overplotted in red, and the transmission is shown in blue, referenced to the right-hand axis. (b–d) Three important spectral contributions to the composite fit: the N_2 LBH bands, where the different vibrational progressions are indicated as is the integrated radiance within the passband; the N_2 VK bands with the vibrational progressions and total radiance indicated; and the N I multiplets with the total radiance for all 10 indicated.

brightest three atomic features as measured in the laboratory under optically thin conditions are fit individually: N II 1085 Å, N I 1134 Å, and N II 916 Å. The other 13 atomic multiplets in the EUV from 862 Å to 1100 Å are fit as one spectral component according to the laboratory-measured relative intensities of *Samson et al.* [1991].

[29] 4. The fourth component is the N_2 Birge-Hopfield I b $^1\Pi_u - X\ ^1\Sigma_g^+$ (1,v″) bands. Although much of this system is highly predissociated, the v′ = 1 progression is not for low J [*Lewis et al.*, 2005a] and the relative intensities of the vibrational bands are taken from the emission cross sections of *James et al.* [1990].

[30] 5. The final component is the H Lyman-β line at 1026 Å.

[31] Since there is not sufficient structure in the CH_4 cross section in the EUV to infer the effective column from the spectral shape, we use the same CH_4 column abundance inferred from FUV analysis for the EUV. EUV CH_4 cross sections are from *Kameta et al.* [2002]. The EUV spectra are therefore fit with the following expression:

$$
\begin{aligned}
D(\lambda, z) = \big[& A_1(z)f_{Ly-\beta}(\lambda) + A_2(z)f_{BHI}(\lambda) \\
& + A_3(z)f_{CY346}(\lambda) + \Sigma_i A_i(z)f_{CY0i}(\lambda) \\
& + \Sigma_j A_j(z)f_{NI}(\lambda) \big] \exp[-N_{CH4}(z)\sigma_{CH4}(\lambda)]
\end{aligned}
\tag{2}
$$

where $f_{Ly-\beta}(\lambda)$ is the shape of the H Lyman-β line, $f_{BHI}(\lambda)$ is the spectrum for the N_2 BH I(1,v″) bands, $f_{CY346}(\lambda)$ is the spectrum for N_2 CY(v′ = 3,4,6), $\Sigma_i f_{CY0i}(\lambda)$ is the sum over the two component fit of the CY(0,0)+CY(0,1) bands and the CY(0,2) band, and $\Sigma_j f_{NIj}(\lambda)$ is the sum over the four separate components of the 16 N I and N II multiplets we fit in the EUV discussed above. The nine A_n coefficients are scalars that are retrieved in the spectral fitting process. As with the FUV, we use the synthetic fit to each spectral component to calculate the radiance contributions at each altitude.

[32] Figures 3a–3d demonstrate the results of this spectral fitting procedure at the same 1000 ± 50 km tangent altitude of Figure 2. Figure 3a shows the composite solution of all components overplotted on the data and the fit is excellent. Also included in Figure 3a is the CH_4 transmission calculated from the effective slant column abundance inferred in Figure 2, referenced to the right-hand axis. It ranges from about 30% on the short wavelength end of the EUV to about 70% on the long wavelength end.

[33] Figures 3b–3d show the components of the composite fit shown in Figure 3a. Figure 3b shows the relative intensities of the N I and N II multiplets produced primarily from photofragmentation as well as the H Lyman-β fit. The N II 1085 Å/N II 916 Å ratio is found to be 6.2 and the N II 1085 Å/N I 1134 Å ratio is 1.4. After accounting for extinction due to CH_4 along the line of sight, these ratios become 3.6 and 1.9, respectively. These are somewhat smaller than the optically thin ratios reported by *Samson et al.* [1991] of 4.4 and 3.5, respectively.

[34] Figure 3c displays the fit to the N_2 CY(3,4,6) progressions as well as the N_2 BH I(1,v″) progression. Most prominent are the blended CY(3,2)+CY(4,3) bands near 945 Å as well as the CY(3,4)+CY(4,5) bands near 985 Å. Wavelengths of the different vibrational bands are indicated in Figure 3c.

[35] Figure 3d gives the fit to the well known CY(0,v″) progression, which is the brightest observed in electron impact laboratory observations [*Zipf and McLaughlin*, 1978; *Ajello et al.*, 1989]. The (0,0) band is optically thick in Titan's atmosphere and absent in the separate disk airglow observations reported by *Ajello et al.* [2007]. This result is in contrast to most Voyager UVS analyses of the Titan airglow which reported that the (0,0) band dominated the EUV. Note that the (0,1)/(0,2) ratio is 1.5, which is in contrast to the optically thin ratio of 10 [*Ajello et al.*, 1989]. We discuss the relative intensities of this important vibrational progression further in section 5.

4. Airglow Modeling: Calculation of EUV and FUV Production Rates

[36] The fitting process described above allows us to retrieve radiances of each feature or progression versus altitude for comparison with predictions using the Atmospheric Ultraviolet Radiance Integrated Code (AURIC) [*Strickland et al.*, 1999; *Stevens*, 2001]. Because there is no clear evidence yet of N_2 airglow emissions observed by UVIS from the dark side of Titan [*Ajello et al.*, 2007], we proceed under the assumption that the airglow is produced exclusively by solar driven processes. AURIC has been used in the analyses of many terrestrial upper atmospheric airglow measurements, including all known emissions arising from photofragmentation and photoelectron excitation of N_2 [*Bishop and Feldman*, 2003]. AURIC uses laboratory-measured excitation cross sections and the solar spectral irradiance to calculate photoelectron fluxes and the resultant VPRs (in $cm^{-3}\ s^{-1}$). From the VPRs we calculate the limb radiances for comparison against the observations, including all known sources of opacity along the line of sight.

[37] We adapt AURIC to Titan's atmosphere by using the shape of the N_2 density profile from the Huygens Atmospheric Structure Instrument (HASI) reported by *Fulchignoni et al.* [2005] but scaled to the N_2 density at 950 km (Orbit T5, $1.32 \times 10^{10}\ cm^{-3}$) from the Ion and Neutral Mass Spectrometer (INMS) reported by *De La Haye et al.* [2007a]. This reduces the reported HASI densities at 950 km by a factor of 3.1 and allows for a smooth description of N_2 densities below the minimum altitude of the INMS. This reduction in densities is crucial to matching the observed altitudes of peak limb radiances between 900 and 1000 km altitude. The HASI N_2 number density profile as well as the INMS profile and the one used in our study are all shown in Figure 4.

[38] We use the solar irradiance measured between 10 and 1050 Å at Earth by the Solar EUV Experiment (SEE, Version 10.02) [*Woods et al.*, 2008; *Lean et al.*, 2011] on 23 June 2009 scaled by $1/R^2$ (R = 9.57 AU) to account for the weaker flux at Titan. There are no solar data available on 22 June so we have taken the data from the following day. The EUV and FUV airglow is controlled by photoelectron excitation and photofragmentation of N_2, which are both initiated by the solar irradiance at wavelengths below 450 Å [*Strickland et al.*, 1995; *Stevens*, 2001; *Bishop and Feldman*, 2003] and this irradiance is shown in Figure 5. While the formal systematic uncertainty for these data is ~30%, use of the SEE data in the AURIC model closely reproduces the terrestrial FUV dayglow observed simulta-
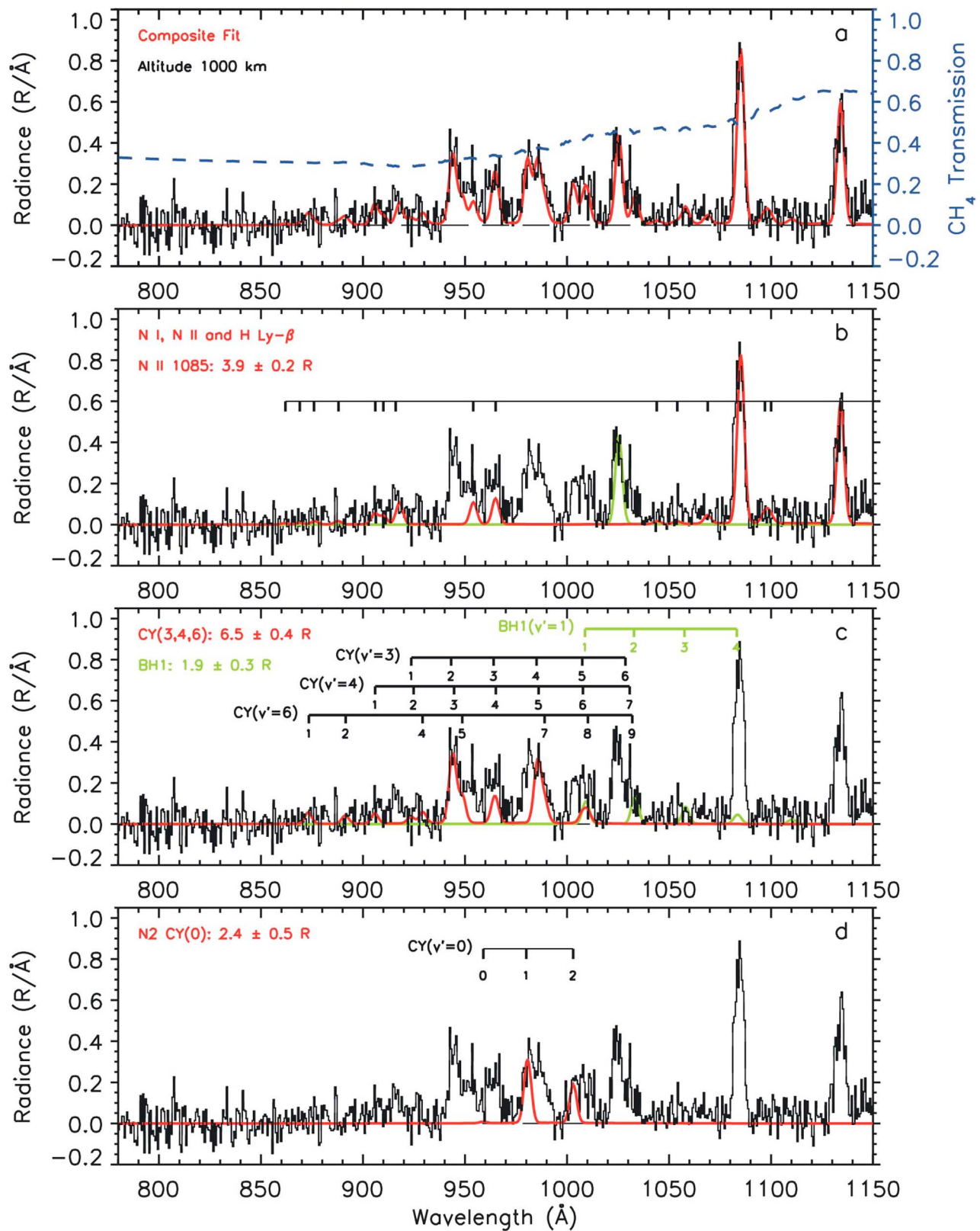
Figure 3. (a) UVIS EUV data from 1000 ± 50 km altitude for the same time period as Figure 2. As in Figure 2, the composite fit is in red, and the transmission is shown in blue. Spectral contributions to the composite fit: (b) the N I and N II multiplets in red and H Lyman-β in green, with the radiance for the brightest N II 1085 Å feature indicated; (c) the N_2 CY(3,4,6) bands as well as the N_2 BH I(1) bands; and (d) the CY(0,v″) bands.
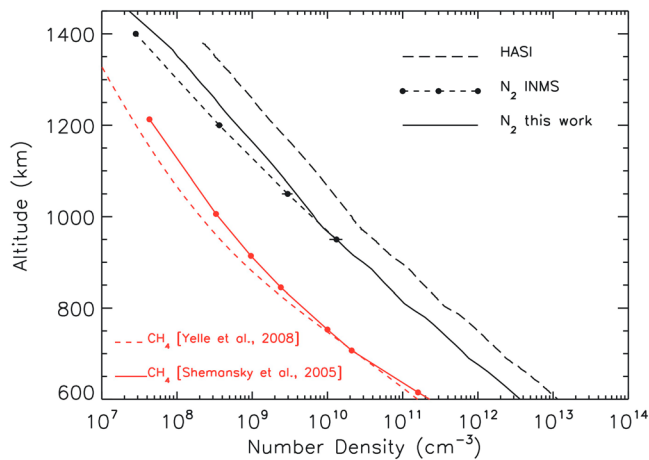
Figure 4. N_2 number density profile reported from the HASI experiment (long-dashed line) and the INMS experiment (short-dashed line). The profile adopted for this study (solid line) is the HASI profile scaled down by a constant factor of 3.1. Also shown are two different CH_4 density profiles from a UVIS occultation [*Shemansky et al.*, 2005] and a model constrained by INMS observations [*Yelle et al.*, 2008].

neously by the GUVI instrument [*Lean et al.*, 2011]. The indicated photon flux ($\lambda < 450$ Å) is a factor of six less than that used in the Voyager 1 UVS EUV airglow analysis of *Stevens* [2001] and reflects the much lower solar activity during the UVIS observational periods.

[39] Using photoionization cross section data from the Photo-Cross Sections and Rate Coefficients database (http://amop.space.swri.edu/) [*Huebner et al.*, 1992], we find that the contribution to the total photoelectron flux from CH_4, which has a mixing ratio of 3% near 1000 km altitude [*De La Haye et al.*, 2007a], to be less than 10% for energies above 5 eV and for altitudes between 900 and 1400 km. The enhanced photoelectron production due to CH_4 results in a 5% or less enhancement in EUV and FUV VPRs under the observed conditions and so we neglect this contribution. We note in passing that it is essential to have precise knowledge of the solar zenith angle (or solar incidence angle) in order to properly compute the extinction of the solar irradiance. We use an average solar incidence angle of 56° for all of our calculations herein (see Figure 1).

[40] Figure 6a shows the calculated photoelectron flux for four different electron energies using the HASI N_2 density profile scaled down by a factor of 3.1 as shown in Figure 4 and the solar spectral irradiance shown in Figure 5. In general, production rates of important solar driven UV airglow emissions peak near 1000 km where most of the XUV solar irradiance is absorbed by the atmosphere. Figure 6b shows the energy spectra of the photoelectron fluxes at four important altitudes for this study. At 1000 km these show a peak between 10^7 and 10^8 electrons $cm^{-2}s^{-1}ev^{-1}$ near 6 eV with a flux about five orders of magnitude less near 100 eV, consistent with the model results of *Lavvas et al.* [2011]. We note, however, that we have adapted our model to N_2 densities reported from INMS measurements rather than those reported by HASI and used by Lavvas

et al. Lower N_2 densities allow for a better fit to the observed radiance profiles discussed in section 5.

[41] Recently, *Young et al.* [2010] remeasured the emission cross sections of the important LBH system in the laboratory and found important differences in magnitude and shape from the previous measurements of *Ajello and Shemansky* [1985]. The new a state emission cross section peak near 20 eV is found to be 26% less than the value from Ajello and Shemansky (after adjustment of the latter cross section for revised calibration). In addition, the cascade contribution from higher lying states is found to be 31% using the a′ and w state excitation cross sections of *Johnson et al.* [2005]. The effective peak emission cross section including cascade is 2.28×10^{-17} cm^2 at 20 eV [*Ajello et al.*, 2010].

5. Airglow Modeling: Comparison of Model Results to UVIS Limb Observations

[42] VPRs from AURIC are used to calculate the radiances of each set of emissions for comparison with the limb observations presented herein. VPRs are interpolated onto a finely spaced altitude grid and integrated explicitly along the line of sight for each tangent altitude under the assumption of spherically symmetric production. Wavelength dependent absorption by CH_4 is included in the calculations using the density profile from UVIS stellar occultation observations and reported by *Shemansky et al.* [2005] (see Figure 4). Calculated limb radiances are then smoothed vertically over 90 km in the FUV and 120 km in the EUV, consistent with the projected field of view of a UVIS pixel in the FUV and the EUV at a line-of-sight distance of 60,000 km.

5.1. FUV Limb Observations

[43] Figure 7 shows VPR vertical profiles and calculated limb radiance profiles compared against observations for all of the emissions arising from solar driven processes on N_2 in the FUV. Figure 7a shows calculated VPRs of the N_2 LBH system, where the peak is 0.8 $cm^{-3}s^{-1}$ at 1005 km. This peak VPR is about a factor of 2.5 less than reported by *Lavvas et al.* [2011], which can probably be attributed to a combination of the new smaller LBH emission cross sections of *Young et al.* [2010] and the lower solar irradiance in June 2009 compared to December 2004 for the disk observations modeled by Lavvas et al. Figure 7b shows the calculated LBH limb radiances within the UVIS passband compared against the observed radiances. The fit is very good and the calculated peak radiance exceeds the data by only 6%, which is within the estimated calibration uncertainty of UVIS (15%). The calculated altitude of peak emission is also in agreement with observations, which provides strong evidence against any magnetospheric source of LBH excitation and also supports the lower INMS N_2 densities. Extinction by CH_4 for the LBH bands is relatively small, as indicated by the dashed line in Figure 7b.

[44] Figure 7c shows calculated VPRs for the N_2 VK system, which include the significant contributions of cascade from higher lying states [*Trajmar et al.*, 1983; *Strickland et al.*, 1999]. Figure 7d shows the corresponding limb radiance profile for the portion of the band sampled by UVIS. Again, the fit to the peak radiances is very good and
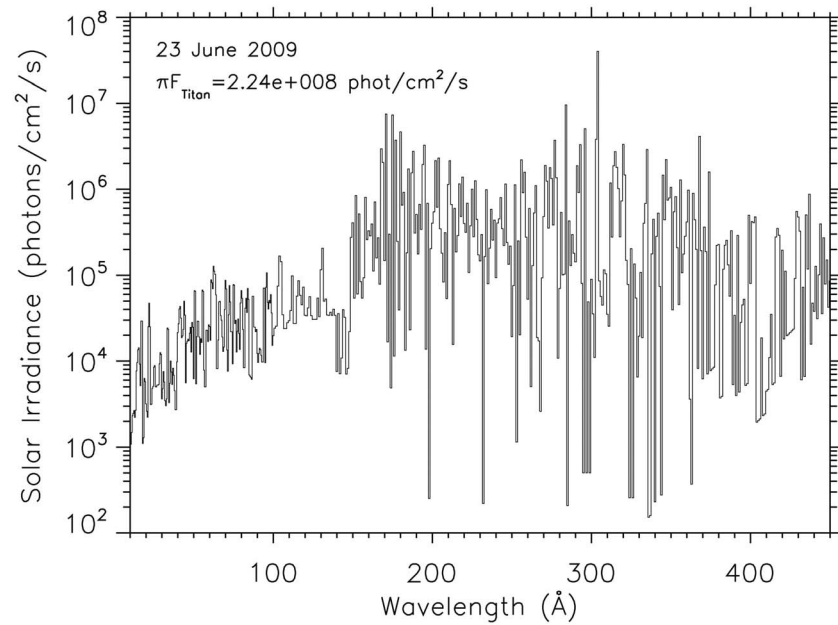
Figure 5. The solar spectral irradiance used in this study. The irradiance at 1 AU [*Lean et al.*, 2011] has been scaled down by a factor of 92 to reflect the smaller irradiance at Titan relative to the Earth. The total indicated (πF_{Titan}) is the irradiance integrated over the spectral region shown (0–450 Å).
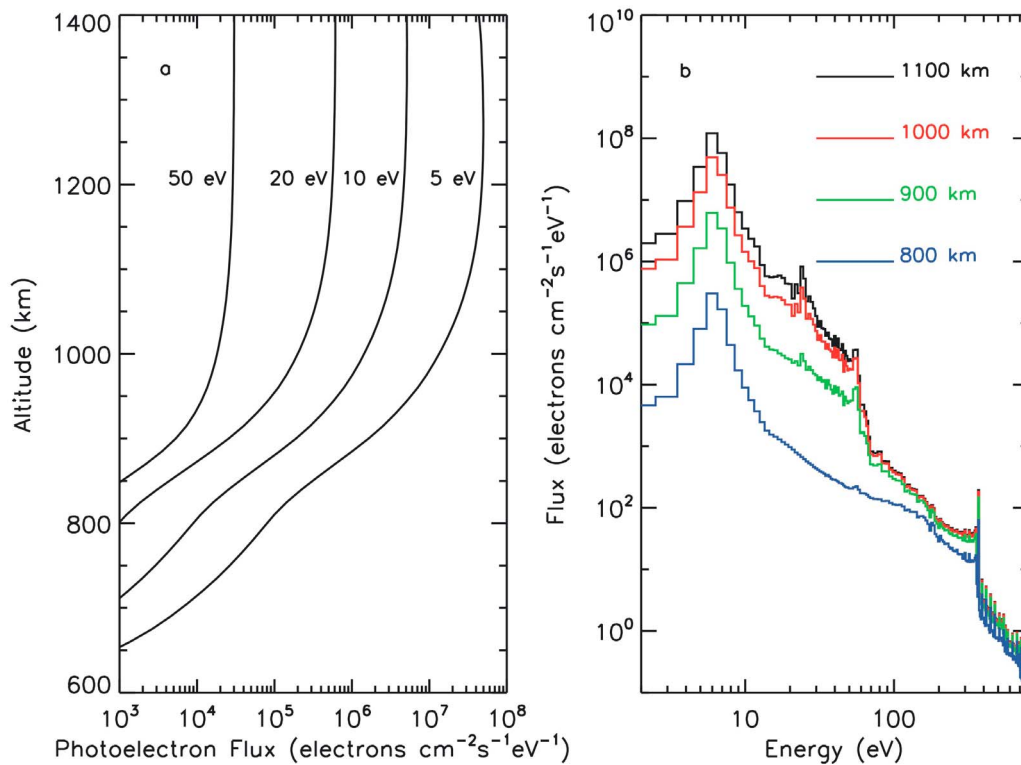

Figure 6. (a) Calculated photoelectron flux versus altitude for several important electron energies using N_2 densities shown in Figure 4 and the solar irradiance shown in Figure 5. (b) Photoelectron energy spectra at four altitudes used in this study.
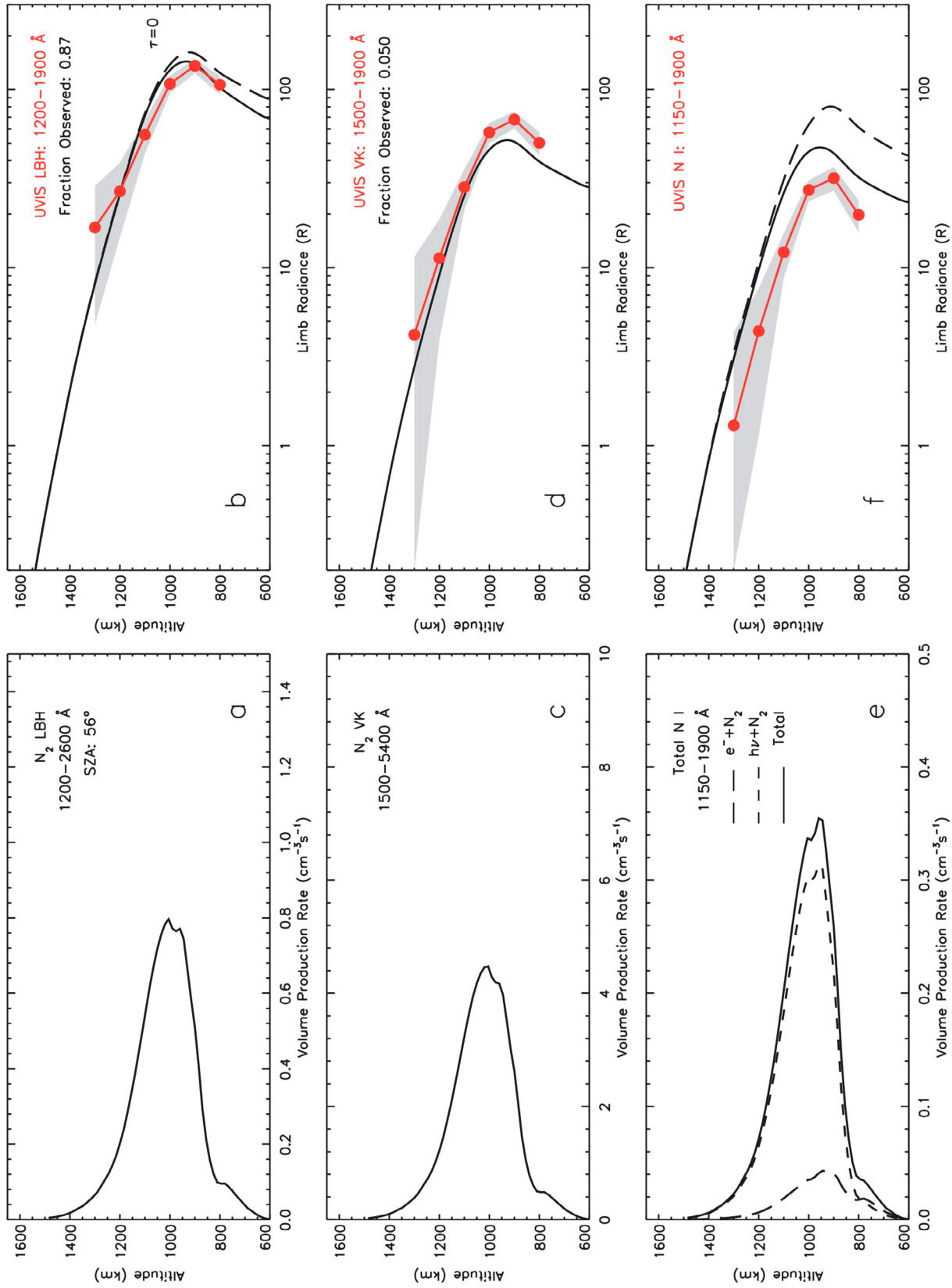
Figure 7

the altitude of peak VK emission also agrees with the observations. The VK bands are not absorbed by CH_4.

[45] Figure 7e shows calculated VPRs for the ten N I multiplets in the FUV, which are dominated by N I 1200 Å and N I 1493 Å (see Figure 2d). The VPRs used to calculate limb radiance are the sum of that from N_2 photofragmentation and photoelectron excitation of N_2. Each of these two contributions are overplotted on Figure 7e, where one can see that photofragmentation dominates the excitation. Emission cross sections from photofragmentation for all N I and N II features in the FUV and EUV have not yet been measured in the laboratory, but we assign emission cross sections to each feature following *Bishop and Feldman* [2003]. Emission cross sections for photoelectron excitation ($N_2 + e \rightarrow N^* + N^{+*}$) are from *James et al.* [1990], *Ajello and Shemansky* [1985], *Stone and Zipf* [1973], and *Mumma and Zipf* [1971]. Using densities reported by *De La Haye et al.* [2007b], we find that direct photoelectron excitation of atomic nitrogen is negligible in the production of the UV airglow. Figure 7f shows the corresponding limb radiances. Although the altitude of the peak emission is again fit well, the predicted emission rate peak is in excess of the observations, which may be due to uncertainties in the emission cross sections used for photofragmentation.

5.2. EUV Limb Observations

[46] Figure 8 shows VPRs and limb radiances for several of the most important airglow emissions in the EUV. Figure 8a shows VPRs for the bright N II 1085 Å feature, where contributions from both photofragmentation and photoelectron excitation are plotted along with the total production. We focus on this EUV multiplet because it is isolated and bright, constituting 40% of the emission from the EUV atomic multiplets at the peak. Figure 8b shows the corresponding limb radiances for this multiplet as well as the limb observations. We find that the predicted peak emission and the peak altitude are in good agreement with the observations. The calculation of N II 1085 Å and the limb radiances for the rest of the features in the EUV is more sensitive to the prescribed CH_4 densities than the FUV calculations, as indicated by the optically thin result overplotted.

[47] Figures 8c and 8d show the VPRs and limb radiances for the N_2 BH I(1) bands. The calculation ignores any multiple scattering effects and uses emission cross sections reported by *James et al.* [1990]. Although these bands have been identified in the terrestrial airglow [e.g., *Gentieu et al.*, 1981; *Chakrabarti et al.*, 1983; *Morrison et al.*, 1990; *Bishop and Feldman*, 2003], a limb scan has not been reported heretofore. Moreover, no reliable model-data comparison has been possible due to blending with adjacent features (see Figure 3). To our knowledge Figure 8d is

therefore the first model-data comparison of the BH I(1) airglow from an N_2 atmosphere.

[48] Figures 8e and 8f show VPRs and limb radiances for the N_2 CY(v' = 3,4,6) progressions. We use the total emission cross section for the CY system reported by *Ajello et al.* [1989] (1.21×10^{-17} cm^2 at 100 eV) scaled down by a factor of 0.164 to represent the emission in CY(v' = 3,4,6). This scaling includes the total from v' = 3 (5.30×10^{-19} cm^2) and v' = 4 (8.25×10^{-19} cm^2) [*Ajello et al.*, 1998] as well as v' = 6 (6.22×10^{-19} cm^2) [*Ajello et al.*, 1989]. We assume that all CY(v' = 3,4,6) bands terminating on the ground vibrational state (v'' = 0) are optically thick so those emission cross sections are not included in our calculations. In addition, many features overlap other CY(v' = 3,4,6) emission bands so that laboratory measured CY(v' = 3,4,6) cross sections cannot easily be quantified [*Ajello et al.*, 1989]. For the v' = 6 progression we have removed the (6,3) and (6,6) bands because they are blended with other features and not identified in higher resolution terrestrial airglow spectra [*Feldman et al.*, 2001]. We have also given 50% of the laboratory measured emission cross section to the blended (6,2) band.

[49] Figure 8f shows that predicted CY(v' = 3,4,6) limb radiances are several times weaker than observations. Figure 8f also shows that even under optically thin conditions the predicted radiances would be less than observed. The inclusion of multiple scattering effects from the v'' = 0 levels would not significantly change this result since emission cross sections to those levels constitute only 14% of the CY(v' = 3,4,6) cross sections used. Misidentification of the bands is unlikely since the composite fit in Figure 3a is extremely good, making it very difficult to identify what else may be contributing to the UVIS spectrum. One possibility in this spectral region is the weaker Birge-Hopfield II (BH II) b'$^1\Sigma_u^+$ − X$^1\Sigma_g^+$ bands [*Ajello et al.*, 1989], but their contribution to the terrestrial airglow is very small relative to other emissions [*Feldman et al.*, 2001]. We discuss the model-data discrepancy in Figure 8f further in section 6.

[50] The CY(0,v'') progression requires a different modeling approach because the resonant (0,0) band near 958 Å has an emission cross section that is 62% of that for the entire CY system and (0,0) is also extremely optically thick in Titan's atmosphere. Photons within this progression are therefore multiply scattered following excitation with their ultimate fate either predissociation or loss as emission in more optically thin bands such as (0,1) near 980 Å and (0,2) near 1003 Å. For this progression we use the multiple scattering model developed for CY(0,v'') in the terrestrial atmosphere [*Stevens et al.*, 1994] and modified for Titan's atmosphere [*Stevens*, 2001]. The input is a plane-parallel model atmosphere and c'$_4$(0) photoelectron excitation rates calculated with AURIC, branching ratios within the progression and relevant absorption cross sections calculated at

Figure 7. VPRs and calculated limb radiances of important FUV emissions at a solar zenith angle of 56°. (a) The VPR vertical profile for the emission in the entire N_2 LBH system and (b) corresponding limb radiances (black). Observed LBH radiances are shown in red (see Figure 2) along with the spectral fitting uncertainty (shaded). The portion of the band used in the comparison (87%) is indicated, as is the optically thin result (dashed line). (c) The VPR for emission in the N_2 VK system and (d) the corresponding limb radiances compared to the data. The portion of the band used (5%) is indicated. (e) The total VPR for all FUV N I multiplets (solid line), where photoelectron excitation and photofragmentation are shown separately, and (f) calculated limb radiance compared to the data.
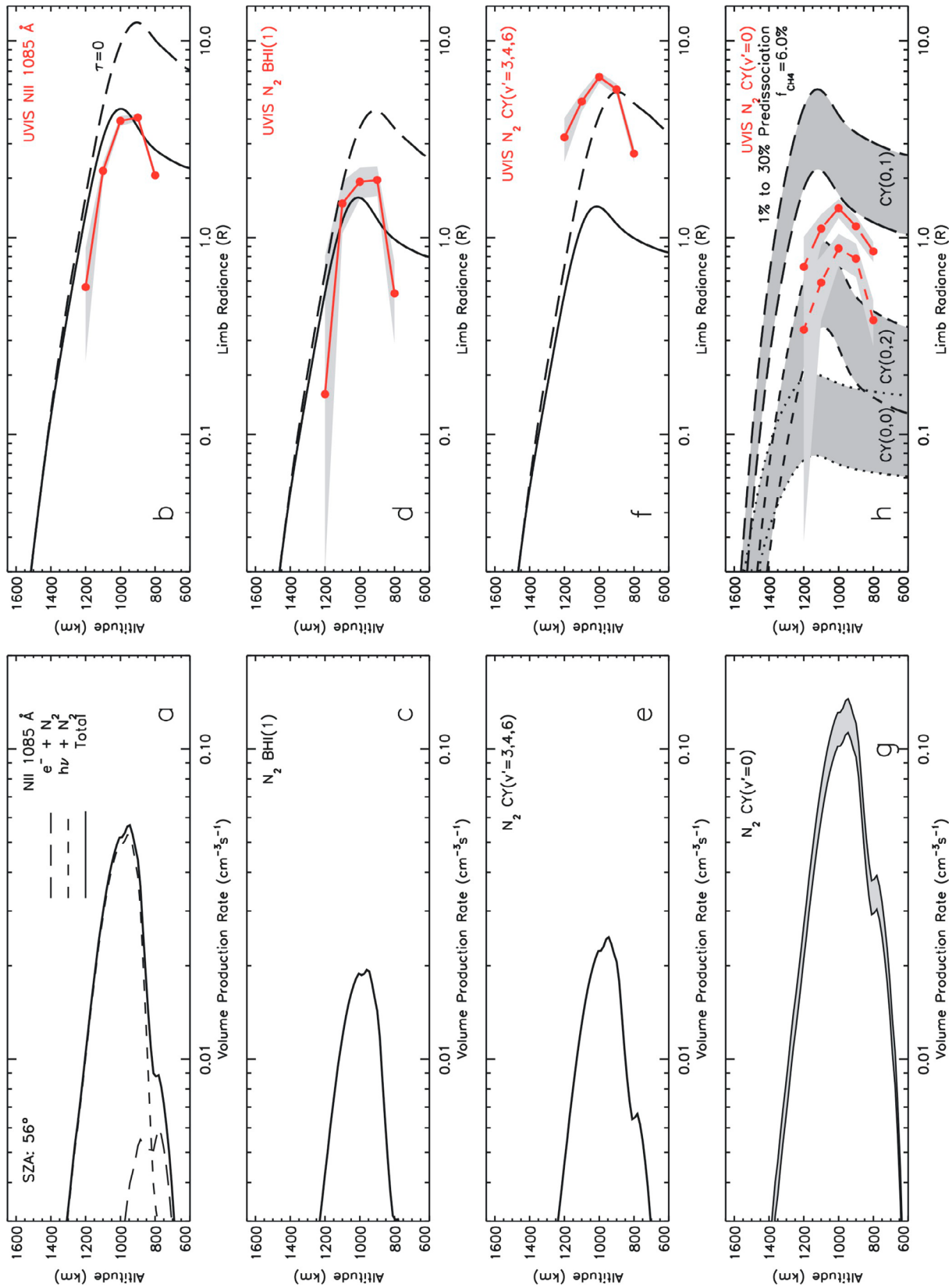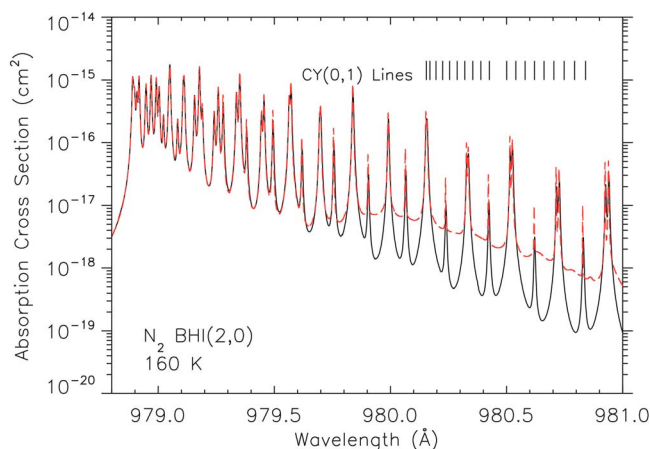
Figure 8

Figure 9. The N_2 coupled channels cross section near the CY(0,1) band at 160 K. Absorption from the BH I(2,0) band used in previous Titan airglow work calculating CY(0,v″) radiances is shown in black. Absorption that includes additional opacity through the C $^3\Pi_u$(v = 8) level and that is used in this work is shown in red. This additional opacity results in more loss within the CY(0,v″) system, where locations of CY(0,1) rotational lines are indicated. The vertical N_2 column abundance near peak photoelectron production is ~1 × 10^{18} cm^{-2} [*Stevens*, 2001].

milliångstrom resolution. This model was used to calculate the terrestrial disk radiances of CY(0,v″) observed by the Far Ultraviolet Spectroscopic Explorer. There, calculated CY(0,1) and CY(0,2) radiances were within 20% of observations [*Bishop et al.*, 2007].

[51] The predissociation branching ratio is an important input to the model because predissociation can be enhanced by a factor of three over its optically thin value through multiple scatterings [*Stevens*, 2001]. Recent work has shown that predissociation within the CY(0,v″) progression has a strong dependence on rotational level with lower levels less predissociated than higher levels [*Shemansky et al.*, 1995; *Ubachs et al.*, 2001]. We herein consider two band averaged predissociation yields of 1% and 30%, which encompass the range of yields reported for the rotational levels populated on Titan [*Liu et al.*, 2005]. Figure 8g shows CY(v′ = 0) VPRs for both 1% and 30% predissociation.

[52] Computation of column emission rates is difficult due to absorption by overlapping N_2 EUV bands. We have shown previously that branching to the CY(0,1) band can result in loss through absorption in the 100% predissociated

BH I(2,0) band, which accidently overlaps the CY(0,1) band [*Stevens et al.*, 1994; *Stevens*, 2001]. An important advance relevant to this problem lies in the ability to calculate accurate N_2 absorption cross sections and predissociation line widths using the coupled channels technique [*Lewis et al.*, 2005b; *Haverd et al.*, 2005]. *Lewis et al.* [2008a] recently experimentally demonstrated enhanced opacity near 980 Å due to the forbidden transition to the C $^3\Pi_u$ (v = 8) level, the transition borrowing strength from the dipole-allowed b-X system through b~C spin-orbit coupling. This contribution had been neglected previously. In this work we have used a coupled channels N_2 model [*Haverd et al.*, 2005; *Lewis et al.*, 2008b] to calculate EUV cross sections for N_2 at a range of relevant temperatures. Figure 9 compares cross sections near 980 Å at 160 K, consistent with temperatures in Titan's upper atmosphere. The comparison shows results from *Stevens* [2001] who neglected the C-X (8,0) band and the coupled channels absorption cross sections that include this band. The location of the CY(0,1) rotational lines are indicated and the enhanced opacities are evident. We include the new cross sections in our multiple scattering model, using upper atmospheric temperatures reported by *Fulchignoni et al.* [2005]. The inclusion of the new cross sections results in about 15% smaller (0,1) peak limb radiances.

[53] Figure 8h compares our multiple scattering model for CY(0,0), CY(0,1) and CY(0,2) with the (0,1) and (0,2) limb observations of UVIS. CY(0,0) is not detectable by UVIS at any tangent altitude. The model calculations include both 1% predissociation (upper limit on radiance) and 30% predissociation (lower limit). Predicted peak (0,2) radiances are in reasonable agreement with UVIS observations, but predicted (0,1) radiances are on average a factor of three larger than observations. For these calculations we use a CH_4 mixing ratio of 6% that is constant with altitude. Varying the CH_4 mixing ratios between 3 and 13% only varies the peak (0,1) radiance between 5 to 7 R for 1% predissociation. We also note that the peak altitude of the predicted CY(0,1) radiances is over 100 km higher than the observed peak altitude (1000 km) and is the only emission feature for which the peak altitude is significantly discrepant. We will discuss these differences next in section 6.

6. Discussion

[54] Table 1 shows a comparison of all of the key FUV and EUV emissions shown in Figures 7 and 8 with observations. Comparisons are for peak brightnesses as well as peak altitudes and differences relative to the observations are shown for each. Most of the observed emission is in the FUV, which

Figure 8. VPRs and calculated limb radiances of important EUV emissions. (a) The VPR vertical profile for the bright N II 1085 Å multiplet calculated, with contributions from photoelectron excitation and photofragmentation plotted separately, and (b) calculated N II 1085 Å limb radiances (solid black line) compared to the observations (red), with the optically thin model result overplotted (dashed black line). (c) VPR for emission in the N_2 BH I(1) progression and (d) BH I(1) limb radiances compared to the observations, analogous to Figure 8b. (e) VPR for emission in the N_2 CY(v′ = 3,4,6) progressions and (f) CY(3,4,6) limb radiances compared to the data. (g) The total VPR for excitation in the N_2 CY(0,v″) progression, which is calculated using both 1% and 30% predissociation of c′$_4$(0) (see text), and (h) calculated limb radiance for CY (0,1) and CY(0,2) using a multiple scattering model compared to the data, where the shaded region represents the results for different amounts of predissociation.

Table 1. Comparison of Modeled and Observed Titan Limb Airglow Radiances

	Observed Peak (R)[a]	Modeled Peak (R)[b]	$\dfrac{\text{Model}}{\text{Observed}}$	Observed Peak (km)	Modeled Peak (km)	Model − Observed (km)
N_2 LBH[c]	136.0 ± 12.5	143.9	1.1	900 ± 55	933	33
N_2 VK[d]	67.8 ± 7.4	52.0	0.8	900 ± 55	928	28
N I[e]	31.8 ± 4.8	47.4	1.5	900 ± 55	956	56
N II 1085 Å	4.1 ± 0.2	4.5	1.1	900 ± 55	996	96
BH I(1)	2.0 ± 0.3	1.6	0.8	900 ± 55	1009	109
CY(3,4,6)	6.5 ± 0.4	1.4	0.2	1000 ± 55	1014	14
CY(0,1)	1.4 ± 0.2	4.2 ± 1.9[f]	3.0	1000 ± 55	1120	120
CY(0,2)	0.9 ± 0.2	0.7 ± 0.3[f]	0.8	1000 ± 55	1080	80

[a]All observations also have a 15% systematic calibration uncertainty that is not shown.
[b]Calculations use a solar incidence angle of 56°, CH_4 densities of *Shemansky et al.* [2005], and N_2 densities shown in Figure 4. Limb radiances are smoothed over 90 km (FUV) or 120 km (EUV), and all model results have a 30% uncertainty due to the XUV solar irradiance used.
[c]Observations and model results represent 87% of the N_2 LBH system.
[d]Observations and model results represent 5% of the N_2 VK system.
[e]Includes all N I features between 1150 and 1900 Å.
[f]Uses 1 to 30% predissociation of the $c'_4(0)$ state and 6% CH_4.

is comprised of the N_2 LBH bands, the N_2 VK bands and N I multiplets. The brightest two UV systems are the LBH and VK, where the total predicted peak radiances are within 5% of the observations and calculated peak altitudes are within uncertainty of the observations, indicating that solar forcing alone can quantitatively explain the observed airglow.

[55] Although the overall agreement between model predictions and the observations is mostly very good, there are some important differences, primarily in the EUV. One significant discrepancy is that the peak brightness for the CY(3,4,6) bands is a factor of five less than the observations. It is unlikely that these emissions are misidentified because higher-resolution terrestrial airglow observations reported by *Feldman et al.* [2001] clearly show the bright CY(3,2)+CY(4,3) bands at 943 Å and the CY(3,4)+CY(4,5) bands at 985 Å without significant blending. Our model calculations of CY(3,4,6) for Titan do not include any contribution to the extinction by overlapping N_2 bands discussed in section 5, which would worsen the discrepancy with observations. We currently have no explanation for the source of this discrepancy, but we note that the CY(3,4,6) bands borrow their intensity from the b′-X levels [*Ajello et al.*, 1989, 1998] and we cannot detect the b′ bands in Titan's airglow. The exchange of intensity between these two systems in the atmosphere of Titan is beyond the scope of this work but is a topic worthy of future study.

[56] Another discrepancy is that the predicted CY(0,1) peak radiance at 980 Å is a factor of three larger than the observations. Although this might suggest a missing source of opacity, we note that the predicted peak altitude is over 100 km higher than observed so that additional opacity would worsen the peak altitude comparison. This is also unlikely because the CY(0,1) band radiances were fit to within 20% in terrestrial airglow data [*Bishop et al.*, 2007]. Additional observations of this important progression would lend critical insight to these differences.

[57] Table 1 also shows that the FUV atomic features arising primarily from photofragmentation are predicted to be 50% larger than the observations. It is unlikely that the solar irradiance used is the source of the discrepancy since the VK bands and the bright LBH bands are fit so well. It is more likely that the emission cross sections used [*Bishop and Feldman*, 2003] are too large. This underscores the

critical need for laboratory measurements of photofragmentation cross sections of N_2 in the EUV and FUV.

[58] We emphasize that limb radiance of many emission features modeled herein are sensitive to the prescribed CH_4 mixing ratio. A comprehensive analysis of the Titan data would result in constraints on the CH_4 abundance. As a first step, we consider the sensitivity of our analysis to two different CH_4 density profiles reported from a UVIS stellar occultation [*Shemansky et al.*, 2005] and from an atmospheric model constrained by INMS observations [*Yelle et al.*, 2008], both of which are shown in Figure 4. We use the N I 1200 Å feature for this sensitivity study; Figure 10a shows the calculated VPRs for this feature. Figure 10b shows the optically thin calculation of the limb radiances as well as the UVIS observations. We remove the calculated CH_4 opacity from the observations using the inferred transmission (see Figure 2a) and scale the optically thin calculation down to this result (a factor of 0.55). This scaling removes any systematic uncertainties from the calculation, such as those from emission cross sections. We then calculate the emergent radiances for the two different CH_4 profiles shown in Figure 4 and find that the larger CH_4 abundances reported by *Shemansky et al.* [2005] are slightly more consistent with our observations of N I 1200 Å. We caution that the Shemansky et al. profile, the Yelle et al. profile, and the airglow data presented here are all based on separate Titan observations so that a variable CH_4 abundance for each set of conditions may well reconcile the discrepant results. Additional observations with latitude and at other times of year would be helpful in this regard. The airglow retrievals are not sensitive to absorption by other hydrocarbons such as acetylene (C_2H_2) and ethane (C_2H_6) due to their relatively low abundances.

[59] A significant finding of this work is that the altitude of peak emission is sensitive to the N_2 densities. Larger N_2 densities from HASI produce an altitude of peak emission 60–70 km higher in Titan's atmosphere, which is inconsistent with the June 2009 peak airglow observations shown in Table 1. Scaling the HASI densities down by a factor of 3.1 is consistent with the INMS (T5) densities at 950 km and yields radiance profiles that are more consistent with the airglow peaks of the different emission features.

[60] The CY(0,1)/CY(0,2) ratio observed by UVIS at peak emission is found to be 1.5 at 1000 km altitude. The optically thin (0,1)/(0,2) ratio is 10 [*Ajello et al.*, 1989], whereas
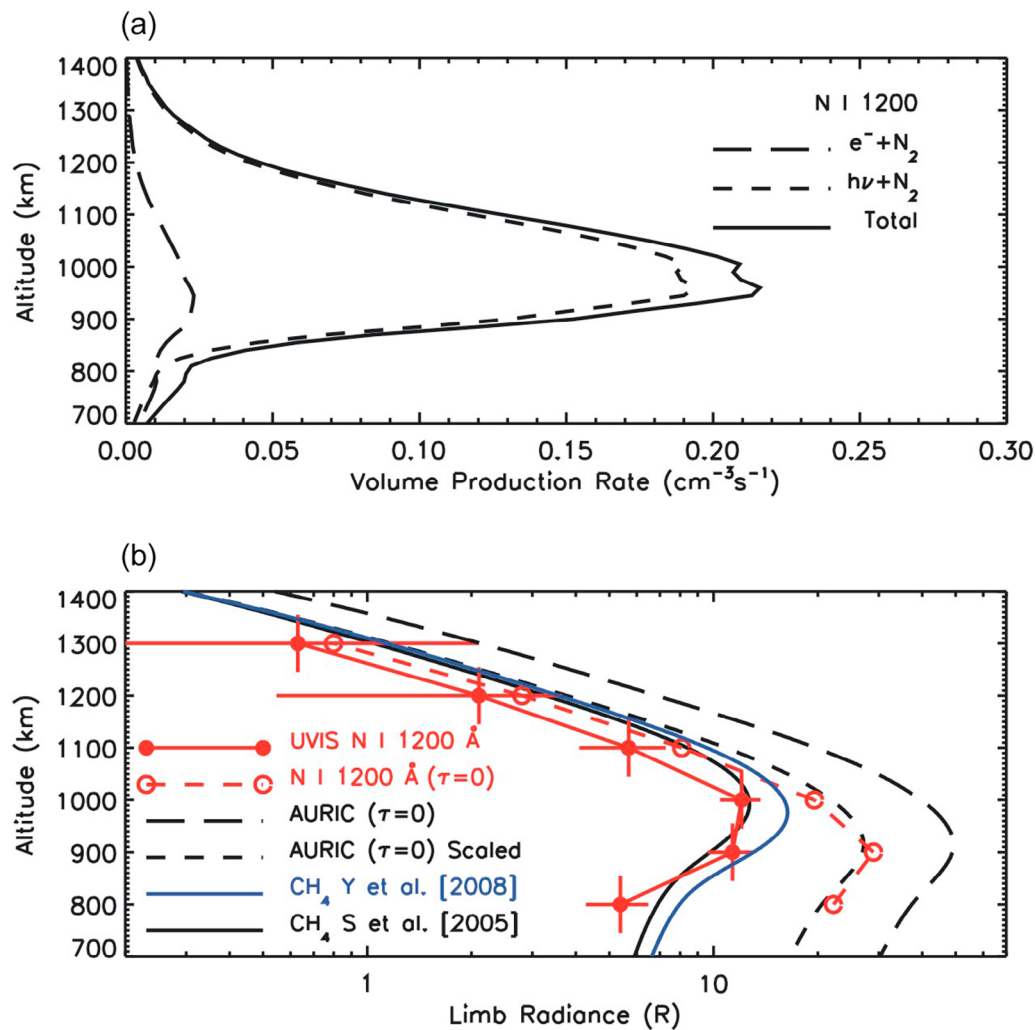
Figure 10. (a) The calculated VPR of the N I 1200 Å feature. (b) Calculated N I 1200 Å optically thin limb radiance (black long-dashed line). The UVIS observations are shown as the solid red line with dots indicating the uncertainty in the measurements. The dashed red line with open circles shows the observed limb emission without CH_4 extinction ($\tau = 0$). We fit the optically thin model result (black long-dashed line) to the optically thin observation using a scale factor of 0.55. The sensitivity of the calculated limb emissions to larger (solid black line [*Shemansky et al.*, 2005]) and smaller (solid blue line [*Yelle et al.*, 2008]) CH_4 densities is shown (see Figure 4).

the predicted ratio is six as a result of the large (0,1) opacities discussed in section 5. The observed ratio of 1.5 cannot be reconciled with variations in the predissociation branching ratio, which affects the (0,1) and (0,2) emissions equally.

7. Summary

[61] We present the highest-quality limb observations of the Titan EUV and FUV airglow to date by UVIS on Cassini from the 22 June 2009 encounter (Cassini orbit T57), which are sufficiently close to Titan to resolve the peak of the emission between 900 and 1000 km for the first time. We find that the spectral content between 750 and 1950 Å consists exclusively of H Lyman-α at 1216 Å, H Lyman-β at 1026 Å and emissions resulting from processes traceable to a N_2 source. We find no C I multiplets in the UVIS FUV

spectra as reported previously [*Ajello et al.*, 2008; *Zhang et al.*, 2010] and instead identify several photoelectron excited N_2 VK bands in the FUV as the likely source of the emission.

[62] We adapt a model for the terrestrial UV airglow to Titan to predict the limb radiances between 800 and 1200 km tangent altitudes. We find that solar driven processes alone can account for the observed radiances, without the need for a supplemental source such as from the magnetosphere. The brightest N_2 systems are the LBH and the VK bands and predicted combined peak radiances for these are within 5% of observations. Although uncertainties in the UVIS calibration (15%) and the estimation of the solar XUV irradiance (30%) allow for a nonsolar contribution of up to 40% at the peak of the LBH and VK bands, the observed peak altitudes and the shape of the FUV and EUV emission profiles in general do not imply a magnetospheric source for

these data. Analysis of additional Cassini encounters with Titan may nonetheless require a magnetospheric source to the airglow, depending on Titan's interaction with Saturn's magnetosphere during the encounter [e.g., *Rymer et al.*, 2009].

[63] Computations of weaker EUV N_2 bands from the CY system disagree with the observations at peak emission. In particular, the CY(3,4,6) bands are overpredicted by a factor of five and the CY(0,1) band is underpredicted by a factor of three. The large disagreement between the HASI and INMS N_2 profile has been clarified by using the sensitivity of the peak emission altitude to the N_2 density profile. We find that the INMS values are consistent with our model-data comparisons. CH_4 densities reported by *Shemansky et al.* [2005] are consistent with the extinction of the UV airglow in our model; other values are unlikely to reconcile the model-data discrepancies in the airglow presented herein. Calculations of FUV N I multiplets produced primarily from photo-fragmentation of N_2 are in excess of observations by 50% underscoring the need for laboratory measured cross sections for this process.

[64] Although the N_2 UV dayside airglow of Titan is far weaker than its terrestrial counterpart [*Bishop and Feldman*, 2003] due to its greater distance from the Sun, the solar driven processes controlling the emergent features from the upper atmosphere are remarkably similar.

References

Ajello, J. M., and D. E. Shemansky (1985), A reexamination of important N_2 cross sections by electron impact with application to the dayglow: The Lyman-Birge-Hopfield band system and N I (119.99 nm), *J. Geophys. Res.*, *90*, 9845–9861, doi:10.1029/JA090iA10p09845.

Ajello, J. M., G. K. James, B. O. Franklin, and D. E. Shemansky (1989), Medium-resolution studies of extreme ultraviolet emission from N_2 by electron impact: Vibrational perturbations and cross sections of the $c'_4 {}^1\Sigma_u^+$ and $b'^1\Sigma_u^+$ states, *Phys. Rev. A*, *40*, 3524–3556, doi:10.1103/PhysRevA.40.3524.

Ajello, J. M., G. K. James, and M. Ciocca (1998), High resolution EUV emission spectroscopy of the N_2 c' ${}^1\Sigma_u^+$ v' = 3 and 4 levels by electron impact, *J. Phys. B At. Mol. Opt. Phys.*, *31*, 2437–2448, doi:10.1088/0953-4075/31/10/028.

Ajello, J. M., et al. (2007), Titan airglow spectra from Cassini Ultraviolet Imaging Spectrograph (UVIS): EUV analysis, *Geophys. Res. Lett.*, *34*, L24204, doi:10.1029/2007GL031555.

Ajello, J. M., et al. (2008), Titan airglow spectra from the Cassini Ultraviolet Imaging Spectrograph: FUV disk analysis, *Geophys. Res. Lett.*, *35*, L06102, doi:10.1029/2007GL032315.

Ajello, J. M., R. S. Mangina, and R. R. Meier (2010), UV molecular spectroscopy from electron impact for applications to planetary atmospheres and astrophysics, in *Charged Particle and Photon Interactions With Matter: Recent Advances, Applications, and Interfaces*, edited by Y. Hatano, Y. Katsumura, and A. Mozumder, chap. 28, Taylor and Francis, Boca Raton, Fla.

Bishop, J., and P. D. Feldman (2003), Analysis of the Astro-1/Hopkins ultraviolet telescope EUV-FUV dayside nadir spectral radiance measurements, *J. Geophys. Res.*, *108*(A6), 1243, doi:10.1029/2001JA000330.

Bishop, J., M. H. Stevens, and P. D. Feldman (2007), Molecular nitrogen Carroll-Yoshino v' = 0 emission in the thermospheric dayglow as seen by

the Far Ultraviolet Spectroscopic Explorer, *J. Geophys. Res.*, *112*, A10312, doi:10.1029/2007JA012389.

Broadfoot, A. L., et al. (1981), Extreme ultraviolet observations from Voyager 1 encounter with Saturn, *Science*, *212*, 206–211, doi:10.1126/science.212.4491.206.

Broadfoot, A. L., et al. (1997), N_2 triplet band systems and atomic oxygen in the dayglow, *J. Geophys. Res.*, *102*, 11,567–11,584, doi:10.1029/97JA00771.

Brune, W. H., G. H. Mount, and P. D. Feldman (1979), Vacuum ultraviolet spectrophotometry and effective temperatures of hot stars, *Astrophys. J.*, *227*, 884–899, doi:10.1086/156798.

Chakrabarti, S., F. Paresce, S. Bowyer, and R. Kimble (1983), The extreme ultraviolet day airglow, *J. Geophys. Res.*, *88*, 4898–4904, doi:10.1029/JA088iA06p04898.

Conway, R. R. (1982), Self-absorption of the N_2 Lyman-Birge-Hopfield bands in the far ultraviolet dayglow, *J. Geophys. Res.*, *87*, 859–866, doi:10.1029/JA087iA02p00859.

De La Haye, V., et al. (2007a), Cassini ion and neutral mass spectrometer data in Titan's upper atmosphere and exosphere: Observation of a suprathermal corona, *J. Geophys. Res.*, *112*, A07309, doi:10.1029/2006JA012222.

De La Haye, V., et al. (2007b), Titan's corona: The contribution of exothermic chemistry, *Icarus*, *191*, 236–250, doi:10.1016/j.icarus.2007.04.031.

Esposito, L. W., et al. (2004), The Cassini Ultraviolet Imaging Spectrograph investigation, *Space Sci. Rev.*, *115*, 299–361, doi:10.1007/s11214-004-1455-8.

Feldman, P. D., D. J. Sahnow, J. W. Kruk, E. M. Murphy, and H. W. Moos (2001), High-resolution FUV spectroscopy of the terrestrial day airglow with the Far Ultraviolet Spectroscopic Explorer, *J. Geophys. Res.*, *106*, 8119–8129, doi:10.1029/2000JA000356.

Fulchignoni, M., et al. (2005), In situ measurements of the physical characteristics of Titan's environment, *Nature*, *438*, 785–791, doi:10.1038/nature04314.

Gan, L., C. N. Keller, and T. E. Cravens (1992), Electrons in the ionosphere of Titan, *J. Geophys. Res.*, *97*, 12,137–12,151, doi:10.1029/92JA00300.

Gentieu, E. P., P. D. Feldman, R. W. Eastes, and A. B. Christensen (1981), Spectroscopy of the extreme ultraviolet dayglow during active solar conditions, *Geophys. Res. Lett.*, *8*, 1242–1245, doi:10.1029/GL008i012p01242.

Haverd, V. E., B. R. Lewis, S. T. Gibson, and G. Stark (2005), Rotational effects in the band oscillator strengths and predissociation linewidths for the lowest ${}^1\Pi_u$—$X^1\Sigma_g^+$ transitions of N_2, *J. Chem. Phys.*, *123*, 214–304, doi:10.1063/1.2134704.

Huber, K. P., and G. Herzberg (1979), *Constants of Diatomic Molecules*, van Nostrand Reinhold, New York.

Huebner, W. F., J. J. Keady, and S. P. Lyon (1992), Solar photo rates for planetary atmospheres and atmospheric pollutants, *Astrophys. Space Sci.*, *195*, 1–294, doi:10.1007/BF00644558.

James, G. K., J. M. Ajello, B. Franklin, and D. E. Shemansky (1990), Medium resolution studies of extreme ultraviolet emission from N_2 by electron impact: The effect of predissociation on the emission cross section of the b ${}^1\Pi_u$ state, *J. Phys. B At. Mol. Opt. Phys.*, *23*, 2055–2081, doi:10.1088/0953-4075/23/12/015.

Johnson, P. V., C. P. Malone, I. Kanik, K. Tran, and M. A. Khakoo (2005), Integral cross sections for the direct excitation of the $A^3\Sigma_u^+$, $B^3\Pi_g$, $W^3\Delta_u$, $B'^3\Sigma_u^-$, $a'^1\Sigma_u^-$, $a^1\Pi_g$, $w^1\Delta_u$, and $C^3\Pi_u$ electronic states in N_2 by electron impact, *J. Geophys. Res.*, *110*, A11311, doi:10.1029/2005JA011295.

Kameta, K., et al. (2002), Photoabsorption, photoionization, and neutral-dissociation cross sections of simple hydrocarbons in the vacuum ultraviolet range, *J. Electron Spectrosc. Relat. Phenom.*, *123*, 225–238, doi:10.1016/S0368-2048(02)00022-1.

Lavvas, P., et al. (2011), Energy deposition and primary chemical products in Titan's upper atmosphere, *Icarus*, in press.

Lean, J. L., et al. (2011), Solar extreme ultraviolet irradiance: Present, past and future, *J. Geophys. Res.*, *116*, A01102, doi:10.1029/2010JA015901.

Lee, A. Y. T., et al. (2001), Enhancement of deuterated ethane on Jupiter, *Astrophys. J.*, *551*, L93–L96, doi:10.1086/319827.

Lewis, B. R., et al. (2005a), Lifetime and predissociation yield of 14N_2 $b^1\Pi_u$(v = 1) revisited: Effects of rotation, *J. Chem. Phys.*, *123*, 236101, doi:10.1063/1.2137722.

Lewis, B. R., et al. (2005b), Predissociation mechanism for the lowest ${}^1\Pi_u$ states of N_2, *J. Chem. Phys.*, *122*, 144302, doi:10.1063/1.1869986.

Lewis, B. R., et al. (2008a), Optical observation of the C, $3s\sigma_g F_3$, and $3p\pi_u G_3$ ${}^3\Pi_u$ states of N_2, *J. Chem. Phys.*, *129*, 164305, doi:10.1063/1.2990655.

Lewis, B. R., et al. (2008b), A coupled-channel model of the ${}^3\Pi_u$ states of N_2: Structure and interactions of the $3s\sigma_g F_3{}^3\Pi_u$ and $3p\pi_u G_3$ ${}^3\Pi_u$ Rydberg states, *J. Chem. Phys.*, *129*, 164306, doi:10.1063/1.2990656.

Liu, X., D. E. Shemansky, M. Ciocca, I. Kanic, and J. M. Ajello (2005), Analysis of the physical properties of the N_2 $c'^1\Sigma_u^+(0)$—$X^1\Sigma_g^-(0)$ transition, *Astrophys. J.*, *623*, 579–584, doi:10.1086/428641.

Morrison, M. D., C. W. Bowers, and P. D. Feldman (1990), The EUV dayglow at high spectral resolution, *J. Geophys. Res.*, *95*, 4113–4127, doi:10.1029/JA095iA04p04113.

Mumma, M. J., and E. C. Zipf (1971), Dissociative excitation of vacuum-ultraviolet emission features by electron impact on molecular gases: 2. N_2, *J. Chem. Phys.*, *55*, 5582–5588, doi:10.1063/1.1675725.

Piper, L. G. (1993), Reevaluation of the transition-moment function and Einstein coefficients for the $N_2(A\ ^3\Sigma_u^+ - X^1\Sigma_g^+)$ transition, *J. Chem. Phys.*, *99*, 3174–3181, doi:10.1063/1.465178.

Rymer, A. M., H. T. Smith, A. Wellbrock, A. J. Coates, and D. T. Young (2009), Discrete classification and electron energy spectra of Titan's varied magnetospheric environment, *Geophys. Res. Lett.*, *36*, L15109, doi:10.1029/2009GL039427.

Samson, J. A. R., Y. Chung, and E.-M. Lee (1991), Excited ionic and neutral fragments produced by dissociation of the N_2^+* H band, *J. Chem. Phys.*, *95*, 717–719, doi:10.1063/1.461424.

Shemansky, D. E. (1969), N_2 Vegard-Kaplan system in absorption, *J. Chem. Phys.*, *51*, 689–700, doi:10.1063/1.1672058.

Shemansky, D. E., I. Kanik, and J. M. Ajello (1995), Fine-structure branching in N_2 c'_4 $^1\Sigma_u^+(0)$, *Astrophys. J.*, *452*, 480–485, doi:10.1086/176320.

Shemansky, D. E., et al. (2005), The Cassini UVIS stellar probe of the Titan atmosphere, *Science*, *308*, 978–982.

Stevens, M. H. (2001), The EUV airglow of Titan: Production and loss of N_2 $c'_4(0)$ − X, *J. Geophys. Res.*, *106*, 3685–3689, doi:10.1029/1999JA000329.

Stevens, M. H., R. R. Meier, R. R. Conway, and D. F. Strobel (1994), A resolution of the N_2 Carroll-Yoshino (c'_4 − X) band problem in the Earth's atmosphere, *J. Geophys. Res.*, *99*, 417–433, doi:10.1029/93JA01996.

Stone, E. J., and E. C. Zipf (1973), Excitation of atomic nitrogen by electron impact, *J. Chem. Phys.*, *58*, 4278–4284, doi:10.1063/1.1678984.

Strickland, D. J., J. S. Evans, and L. J. Paxton (1995), Satellite remote sensing of thermospheric O/N_2 and solar EUV: 1. Theory, *J. Geophys. Res.*, *100*, 12,217–12,226, doi:10.1029/95JA00574.

Strickland, D. J., et al. (1999), Atmospheric Ultraviolet Radiance Integrated Code (AURIC): Theory, software architecture, inputs, and selected results, *J. Quant. Spectrosc. Radiat. Transfer*, *62*, 689–742, doi:10.1016/S0022-4073(98)00098-3.

Strobel, D. F., and D. E. Shemansky (1982), EUV emission from Titan's upper atmosphere: Voyager 1 encounter, *J. Geophys. Res.*, *87*, 1361–1368, doi:10.1029/JA087iA03p01361.

Strobel, D. F., R. R. Meier, and D. J. Strickland (1991), Nitrogen airglow sources: Comparison of Triton, Titan, and Earth, *Geophys. Res. Lett.*, *18*, 689–692, doi:10.1029/91GL00133.

Strobel, D. F., M. E. Summers, and X. Zhu (1992), Titan's upper atmosphere: Structure and ultraviolet emissions, *Icarus*, *100*, 512–526, doi:10.1016/0019-1035(92)90114-M.

Trajmar, S., D. F. Register, and A. Chutjian (1983), Electron scattering by molecules II. Experimental methods and data, *Phys. Rep.*, *97*, 219–356, doi:10.1016/0370-1573(83)90071-6.

Ubachs, W., et al. (2001), Lifetime measurements on the $c'^1_4\Sigma_u^+$, v = 0, 1 and 2 states of molecular nitrogen, *Chem. Phys.*, *270*, 215–225, doi:10.1016/S0301-0104(01)00378-0.

Woods, T. N., et al. (2008), XUV Photometer System (XPS): Improved solar irradiance algorithm using CHIANTI spectral models, *Sol. Phys.*, *250*, 235–267, doi:10.1007/s11207-008-9196-6.

Yelle, R. V., J. Cui, and I. C. F. Müller-Wodarg (2008), Methane escape from Titan's atmosphere, *J. Geophys. Res.*, *113*, E10003, doi:10.1029/2007JE003031.

Young, J. A., et al. (2010), Lyman-Birge-Hopfield emissions from electron-impact excited N_2, *J. Phys. B At. Mol. Opt. Phys.*, *43*, 135201, doi:10.1088/0953-4075/43/13/135201.

Zhang, X., J. M. Ajello, and Y. L. Yung (2010), Atomic carbon in the upper atmosphere of Titan, *Astrophys. J.*, *708*, L18–L21, doi:10.1088/2041-8205/708/1/L18.

Zipf, E. C., and R. W. McLaughlin (1978), On the dissociation of nitrogen by electron impact and by EUV photo-absorption, *Planet. Space Sci.*, *26*, 449–462, doi:10.1016/0032-0633(78)90066-1.

J. M. Ajello, Jet Propulsion Laboratory, California Institute of Technology, Pasadena, CA 91109, USA.

E. T. Bradley, Department of Physics, University of Central Florida, Orlando, FL 32816, USA.

L. W. Esposito, G. Holsclaw, W. E. McClintock, and A. I. F. Stewart, Laboratory for Atmospheric and Space Physics, University of Colorado at Boulder, Boulder, CO 80303, USA.

J. S. Evans and A. J. Kochenash, Computational Physics, Inc., Springfield, VA 22151, USA.

J. Gustin, Laboratoire de Physique Atmosphérique et Planétaire, Université de Liège, B-4000 Liège, Belgium.

A. N. Heays and B. R. Lewis, Research School of Physics and Engineering, Australian National University, Canberra, ACT 0200, Australia.

R. R. Meier, Department of Physics and Astronomy, George Mason University, Fairfax, VA 22030, USA.

A. W. Stephan and M. H. Stevens, Space Science Division, Naval Research Laboratory, Washington, DC 20375, USA. (michael.stevens@nrl.navy.mil)